Influence of Linear Depth Variation on Poincaré, Kelvin, and Rossby Waves

A. N. STANIFORTH

Recherche en Prévision Numérique, Atmospheric Environment Service, Dorval, Quebec, Canada

R. T. WILLIAMS

Department of Meteorology, Naval Postgraduate School, Monterey, California

B. NETA

Department of Mathematics, Naval Postgraduate School, Monterey, California

(Manuscript received 12 April 1991, in final form 11 May 1992)

ABSTRACT

Exact solutions to the linearized shallow-water equations in a channel with linear depth variation and a mean flow are obtained in terms of confluent hypergeometric functions. These solutions are the generalization to finite s (depth variation parameter) of the approximate solutions for infinitesimal s. The equations also respect an energy conservation principle (and the normal modes are thus neutrally stable) in contradistinction to those of previous studies. They are evaluated numerically for a range in s from $s = 0.1$ to $s = 1.95$, and the range of validity of previously derived approximate solutions is established. For small s the Kelvin and Poincaré solutions agree well with those of Hyde, which were obtained by expanding in s. For finite s the solutions differ significantly from the Hyde expansions, and the magnitude of the phase speed decreases as s increases. The Rossby wave phase speeds are close to those obtained when the depth is linearized although the difference increases with s. The eigenfunctions become more distorted as s increases so that the largest amplitude and the smallest scale occur near the shallowest boundary. The negative Kelvin wave has a very unusual behavior as s increases.

1. Introduction

The shallow-water equations are frequently used in simplified dynamical studies of atmospheric and oceanographic phenomena. When the equations are linearized, the thickness of the fluid is often assumed to be a linear function of one of the spatial coordinates. Also, the motion is usually confined to a channel so that the percentage variation of the thickness can be kept small. The thickness variation may come from free-surface slope associated with a constant geostrophic current or linear variation in bottom topography. In most studies, equations with constant coefficients are obtained by making the depth constant except where it is differentiated (for example, see Pedlosky 1979). While this considerably simplifies the analysis, it also leads to two weaknesses. First it restricts the validity of the results to small s, and second it violates the energy conservation principle of the problem. Hyde (1984) studied Kelvin and Poincaré waves with linear depth variations by using an asymptotic expansion to represent the effects of the depth variation.

In this paper we will obtain solutions to the linearized shallow-water equations with the full linear variation in depth included. In particular, the percentage variation of the depth will not be assumed to be small. These solutions will be compared with previously derived approximate solutions to establish their range of validity.

2. Basic equations

The basic equations for this study are derived in Pedlosky (1979, section 3.6). The thickness of the fluid layer is expressed

$$H(x, y, t) = H_0(y) + \eta(x, y, t), \qquad (2.1)$$

where it is assumed that $|\eta| \ll H$. If u and v are small velocity perturbations, the equations of motion become

$$\frac{\partial u}{\partial t} - fv = -g\frac{\partial \eta}{\partial x}, \qquad (2.2)$$

$$\frac{\partial v}{\partial t} + fu = -g\frac{\partial \eta}{\partial y}. \qquad (2.3)$$

The continuity equation is written

$$\frac{\partial \eta}{\partial t} + H_0\frac{\partial u}{\partial x} + \frac{\partial}{\partial y}(vH_0) = 0. \qquad (2.4)$$

Corresponding author address: Dr. R. T. Williams, Department of the Navy, Naval Postgraduate School, Department of Meteorology, Monterey, CA 93943-5100.

In this set of equations there is no mean current, and the thickness variation $H_0(y)$ comes entirely from the sloping bottom. A mean current U could be added that would lead to a geostrophically balanced free-surface slope. However, with no loss of generality, we can neglect the mean current, since [see Hyde (1984) and the following] we can recover the mean current by simply redefining a slope parameter and by Doppler shifting a phase speed in the no-mean current solution.

The system (2.2)–(2.4) is combined to give the following equation for η:

$$\frac{\partial}{\partial t}\left[\left(\frac{\partial^2}{\partial t^2}+f^2\right)\eta-\nabla\cdot(gH_0(y)\nabla\eta)\right]+gf\frac{\partial H_0}{\partial y}\frac{\partial\eta}{\partial x}=0. \quad (2.5)$$

After η is determined, the velocity components can be obtained from these relations:

$$\left(\frac{\partial^2}{\partial t^2}+f^2\right)u=-g\left(\frac{\partial^2\eta}{\partial x\partial t}+f\frac{\partial\eta}{\partial y}\right), \quad (2.6)$$

$$\left(\frac{\partial^2}{\partial t^2}+f^2\right)v=-g\left(\frac{\partial^2\eta}{\partial y\partial t}-f\frac{\partial\eta}{\partial x}\right). \quad (2.7)$$

The linear variation of H_0 in y is written

$$H_0=D_0\left(1-\frac{sy}{L}\right), \quad (2.8)$$

where D_0 is the value at $y=0$. The rigid walls are placed at $y=\pm L/2$. When a wave solution of the form

$$\eta=\mathcal{R}\phi(y)\exp[ik(x-ct)] \quad (2.9)$$

is introduced into (2.5), we obtain the equation

$$\left(1-\frac{sy}{L}\right)\frac{d^2\phi}{dy^2}-\frac{s}{L}\frac{d\phi}{dy}+\left[\frac{k^2c^2-f^2}{gD_0}-\frac{fs}{Lc}-k^2\left(1-\frac{sy}{L}\right)\right]\phi=0. \quad (2.10)$$

The boundary condition that v vanishes along $y=\pm L/2$ is applied in (2.7), which with the use of (2.9) gives

$$\frac{d\phi}{dy}+\frac{f}{c}\phi=0, \quad y=\pm\frac{L}{2}. \quad (2.11)$$

Equation (2.10) subject to the boundary conditions (2.11) constitutes the eigenvalue problem for c. In appendix A it is shown that the eigenvalue c must be real and therefore all of the normal modes are neutrally stable. This is a manifestation of the conservation of integrated perturbation energy $E=\iint\{[gH_0(u^2+v^2)+(g\eta)^2]/2\}dxdy$, a result that can be obtained by multiplying (2.2)–(2.4) by gH_0u, gH_0v, and $g^2\eta$, respectively; adding the results; integrating over the domain; and applying the channel boundary conditions. Note that making the depth constant everywhere except where it is differentiated, as in Pedlosky (1979) and Hyde (1984), leads to $dE/dt=gD_0(s/L)\iint g\times\eta vdxdy\neq 0$.

In other words, the normal modes no longer respect the energy conservation principle of the problem, and this assumption changes the nature of the solution: modes that should be neutrally stable may become either unstable or damped. This result is consistent with the neglect of a term of $O(s/L)$ in the equations and merely says that the energy is conserved only to $O(s/L)$. Nevertheless it is somewhat worrisome in the sense that it changes a fundamental stability property of the problem and opens up the possibility that the range of validity of the solution of the resulting approximate problem may be unduly limited.

Hyde (1984) has pointed out that the solutions can be generalized to include a mean current U if c is replaced by $c-U$, and s by

$$s+\frac{fUL}{gD_0}.$$

Pedlosky (1979, section 3.10) has obtained solutions for Poincaré, Kelvin, and Rossby waves by assuming $s\ll 1$ in (2.10). Hyde (1984) has also computed the $O(s)$ correction to the Poincaré and Kelvin waves. In our study we will not restrict s to be small; we will require only that H_0 remains positive in the domain. Robinson (1964) obtained solutions to (2.10) in terms of Bessel functions by assuming that $k^2L^2\ll 1$ and $f^2L^2\ll gD_0$. For his application to shelf waves he matched to an outer flat-bottom solution. Saint-Guily (1976) solved a similar problem in which the continental shelf depth variation was represented with a hyperbolic tangent dependence. The solutions were obtained in terms of hypergeometric functions. The eigenfunctions for the free surface height had a maximum over the upper part of the steep bottom slope.

3. Analytic solution of the eigenproblem

It is convenient to rewrite the eigenproblem in the form

$$\mathcal{L}\phi-\lambda(c)\phi=0, \quad (3.1)$$

$$\frac{d\phi}{dy}+\frac{1}{c}f\phi=0, \quad y=\pm\frac{L}{2}, \quad (3.2)$$

where the linear self-adjoint operator $\mathcal{L}$ is

$$\mathcal{L}=-\frac{d}{dy}\left[\left(1-\frac{s}{L}y\right)\frac{d}{dy}\right]+k^2\left(1-\frac{s}{L}y\right), \quad (3.3)$$

and

$$\lambda(c)=\frac{k^2c^2-f^2}{gD_0}-\frac{fs}{Lc}. \quad (3.4)$$

What makes this problem more difficult than the

usual textbook problem is that λ in (3.1) is constrained to have a particular functional dependence [given by (3.4)] on c, which also appears in the boundary conditions (3.2). The dependence of the boundary conditions on c will not allow us to use the theory in Stakgold (1979, pp. 411–418).

A simple linear transformation

$$z = 2k\left(\frac{L}{s} - y\right) \tag{3.5}$$

leads to

$$\frac{d}{dz}\left(z\frac{d\phi}{dz}\right) - \left(\frac{z}{4} - \frac{\lambda(c)L}{2sk}\right)\phi = 0, \quad z_- < z < z_+, \tag{3.6}$$

$$\frac{d\phi}{dz} - \frac{1}{c}\frac{f}{2k}\phi = 0, \quad z = z_\pm, \tag{3.7}$$

where

$$z_- = \frac{2kL}{s}\left(1 - \frac{s}{2}\right), \tag{3.8}$$

$$z_+ = \frac{2kL}{s}\left(1 + \frac{s}{2}\right). \tag{3.9}$$

Equation (3.6) can be transformed to Kummer's equation (e.g., see Abramowitz and Stegun 1965, pp. 504–515) using

$$\phi = \exp\left(\frac{-z}{2}\right)\psi. \tag{3.10}$$

The boundary value problem [(3.6)–(3.7)] becomes

$$z\frac{d^2\psi}{dz^2} + (1 - z)\frac{d\psi}{dz} - \left(\frac{1}{2} - \frac{\lambda(c)L}{2sk}\right)\psi = 0, \tag{3.11}$$

$$\frac{d\psi}{dz} - \frac{1}{2}\left(1 + \frac{1}{c}\frac{f}{k}\right)\psi = 0. \quad z = z_\pm. \tag{3.12}$$

The general solution of (3.11) is

$$\psi(z) = A\psi_1(z) + B\psi_2(z), \tag{3.13}$$

where

$$\psi_1(z) = \begin{cases} M(a(c), 1; z_\pm), & a(c) \neq -n \\ L_n(z), & a(c) = -n, \end{cases} \tag{3.14}$$

$$\psi_2(z) = \begin{cases} U(a(c), 1; z_\pm), & a(c) \neq -n \\ \ln|z|L_n(z) + \sum_{m=1}^{\infty} b_m z^m, & a(c) = -n, \end{cases} \tag{3.15}$$

and

$$a(c) = \frac{1}{2} - \frac{\lambda(c)L}{2sk}. \tag{3.16}$$

The functions M and U are called confluent hypergeometric functions, and $L_n(z)$ is the Laguerre polynomial of degree n. For properties of these functions, recurrence relations, derivatives, and special cases see, for example, Abramowitz and Stegun (1965).

The parameters A, B can be specified by using the boundary conditions (3.12); that is,

$$A\left[\frac{d\psi_1(z_\pm)}{dz} - q(c)\psi_1(z_\pm)\right] + B\left[\frac{d\psi_2(z_\pm)}{dz} - q(c)\psi_2(z_\pm)\right] = 0, \tag{3.17}$$

where

$$q(c) = \frac{1}{2}\left(1 + \frac{1}{c}\frac{f}{k}\right). \tag{3.18}$$

Note that

$$\frac{dM(a(c), 1; z)}{dz} = a(c)M(a(c) + 1, 2; z), \tag{3.19}$$

$$\frac{dU(a(c), 1; z)}{dz} = -a(c)U(a(c) + 1, 2; z), \tag{3.20}$$

$$\frac{dL_n(z)}{dz} = \sum_{m=1}^{n} m(-1)^m\binom{n}{n-m}\frac{1}{m!}z^{m-1}, \tag{3.21}$$

and

$$\frac{d(\ln|z|L_n(z) + \sum_{m=1}^{\infty} b_m z^m)}{dz} = \frac{1}{z}L_n(z) + \ln|z|\frac{dL_n(z)}{dz} + \sum_{m=1}^{\infty} m b_m z^{m-1}. \tag{3.22}$$

Thus, the eigenvalues c are the solutions of

$$\begin{aligned}&[aM(a + 1, 2; z_+) - qM(a, 1; z_+)] \\ &\times [-aU(a + 1, 2; z_-) - qU(a, 1; z_-)] \\ &- [aM(a + 1, 2; z_-) - qM(a, 1; z_-)] \\ &\times [-aU(a + 1, 2; z_+) - qU(a, 1; z_+)] \\ &= 0\end{aligned} \tag{3.23}$$

if $a(c) \neq -n$. For negative integer values of $a(c)$, (3.23) becomes

$$\ln\frac{|z_-|}{|z_+|}C_+C_- + C_+D_+ - C_-D_- = 0, \tag{3.24}$$

where

$$C_\pm = L_n'(z_\pm) - q(c)L_n(z_\pm) \tag{3.25}$$

$$D_\pm = \frac{L_n(z_\pm)}{z_\pm} + \sum_{m=0}^{\infty}[(m + 1)b_{m+1} - q(c)b_m]z_\pm^m. \tag{3.26}$$

The confluent hypergeometric function $M(a, 1; z)$ has a particularly simple form when $a = 0$ and 1, namely, $\exp(z)$ and 1, respectively. It turns out that $a = 0$ when $c = -f/k$ and $a = 1$ when $c = +f/k$, and that $[aM(a + 1, 2; z) - qM(a, 1; z)]$ is identically zero for both cases [note that $M(2, 2; z) \equiv M(1, 1; z)$]. Consequently, $c = f/k$ and $c = -f/k$ are both eigenvalues [since (3.23) is satisfied], and the corresponding eigenfunctions are $\exp(-ky)$ and $\exp(ky)$, respectively. However, it is shown in appendix B that inertial oscillations are possible only if k satisfies the constraint (B.10), and this is a consequence of the singularities of the operator $(\partial^2/\partial t^2 + f^2)$ appearing in (2.5)–(2.7). For zero s, (B.10) reduces to $k = \pm R^{-1}$, the inertial oscillation discussed in Pedlosky (1979, section 3.9), which is indistinguishable at that wavenumber from a Kelvin wave. In general (B.10) will not be satisfied, and therefore the inertial eigenvalues are spurious in the context of the original meteorological problem.

Computer subroutines were developed for stably evaluating the confluent hypergeometric functions $M(a, b; z)$ and $z^a U(a, b; z)$ based on the recurrence relations as suggested by Wimp (1984, pp. 61–64). These subroutines were combined with a zero-finding routine to obtain the values of c satisfying (3.23). For those eigenvalues c_m, one computes the eigenfunctions ψ_m by

$$\psi_m = A(c_m)M(a(c_m), 1; z) + B(c_m)U(a(c_m), 1; z), \tag{3.27}$$

where

$$A(c_m) = -a(c_m)U(a(c_m) + 1, 2; z_+) - q(c_m)U(a(c_m), 1; z_+), \tag{3.28}$$

$$B(c_m) = -a(c_m)M(a(c_m) + 1, 2; z_+) - q(c_m)U(a(c_m), 1; z_+). \tag{3.29}$$

Another way of obtaining the eigenvalues is by numerically solving the boundary value problem (3.1)–(3.2). It turns out that the numerical scheme is not as computationally intensive as the foregoing procedure. However, the analytic solution is useful in asymptotic analysis in other investigations.

4. Numerical solutions of the eigenproblem

In this section we discuss the numerical solution of (3.6)–(3.7) in order to examine the case where $a = -n$. Let us write the equations as follows:

$$\frac{d}{dz}\left(z\frac{d\phi}{dz}\right) - \left(\frac{z}{4} + \mu\right)\phi + c^2\rho\phi - \frac{1}{c}\delta\phi = 0, \quad z_- \leq z \leq z_+ \tag{4.1}$$

$$\frac{d\phi}{dz} - \frac{1}{c}\delta\phi = 0 \quad z = z_\pm, \tag{4.2}$$

where

$$\mu = \frac{f^2 L}{2skgD_0}, \tag{4.3}$$

$$\rho = \frac{kL}{2sgD_0}, \tag{4.4}$$

$$\delta = \frac{f}{2k}. \tag{4.5}$$

Divide the interval $[z_-, z_+]$ into $N - 1$ subintervals by the equally spaced points

$$z_i = z_- + (i - 1)h, \quad i = 1, 2, \cdots, N, \tag{4.6}$$

where

$$h = \frac{z_+ - z_-}{N - 1}. \tag{4.7}$$

Since the eigenvalues c_m are real (see appendix A), we approximate Eq. (4.1) by

$$\frac{z_{i+1}(\phi_{i+1} - \phi_i) - z_i(\phi_i - \phi_{i-1})}{h^2} - \left(\frac{z_i}{4} + \mu\right)\phi_i + c^2\rho\phi_i - \frac{1}{c}\delta\phi_i = 0, \quad i = 2, 3, \cdots, N - 1, \tag{4.8}$$

and the boundary conditions by

$$\frac{\phi_2 - \phi_1}{h} - \frac{1}{c}\delta\phi_1 = 0, \tag{4.9}$$

$$\frac{\phi_N - \phi_{N-1}}{h} - \frac{1}{c}\delta\phi_N = 0, \tag{4.10}$$

where $\phi_i = \phi(z_i)$. This system can be written in matrix form as

$$\mathbf{A}\vec{\phi} + \frac{1}{c}\mathbf{D}^1\vec{\phi} + c^2\mathbf{D}^2\vec{\phi} = 0, \tag{4.11}$$

where $\mathbf{D}^1$, $\mathbf{D}^2$ are diagonal matrices with

$$D^1_{ii} = \begin{cases} -\delta, & i = 2, \cdots, N - 1 \\ -\delta z_2/h, & i = 1 \\ \delta z_N/h, & i = N \end{cases} \tag{4.12}$$

$$D^2_{ii} = \begin{cases} 0, & i = 1, N \\ \rho, & i = 2, \cdots, N - 1 \end{cases} \tag{4.13}$$

and $\mathbf{A}$ is a symmetric tridiagonal matrix whose diagonal elements are

$$a_{ii} = \begin{cases} z_2/h^2 & i = 1 \\ (z_i + z_{i+1})/h^2 + z_i/4 + \mu & i = 2, \cdots, N - 1 \\ z_N/h^2 & i = N, \end{cases} \tag{4.14}$$

and the superdiagonal elements are given by

$$a_{ii+1} = -\frac{z_i}{h^2}, \quad i = 1, 2, \cdots, N-1. \quad (4.15)$$

The eigenvalues were computed by solving

$$\det\left(-\mathbf{A} + \frac{1}{c}\mathbf{D}^1 + c^2\mathbf{D}^2\right) = 0 \quad (4.16)$$

using LINPACK to evaluate the determinant of a tridiagonal matrix in a banded storage mode. This allows us to use $N = 1500$. The eigenvalues are computed for various values of s, in double precision on an IBM3033 computer.

These numerically computed eigenvalues agree with those computed from the analytic solutions (3.23)–(3.24) of section 3.

5. Phase speeds

When interpreting the results, it should be borne in mind that s is large not only when the bottom slope is large. This is because s can also be large when mean advection is included (see section 2) in which case s is replaced by $s + fUL/(gD_0)$. In other words, large values of s are not only obtained when the bottom slope is large but also when the mean current and channel width are large and the depth (or equivalent height) is small. Therefore a large fixed value of s can be entirely due to a large bottom slope, entirely due to a large value of $fUL/(gD_0)$, or to a combination of the two extremes. It is particularly important to bear this in mind when interpreting results as a function of scale. Before presenting the new results, the simplified formulas from Pedlosky (section 3.6, 1979) will be given. Phase speeds of the Poincaré waves that are obtained by setting $s = 0$ are

$$c = \pm\left[\left(k^2 + \frac{n^2\pi^2}{L^2}\right)gD_0 + f^2\right]^{1/2}. \quad (5.1)$$

The eigenfunctions are sinusoidal functions of y with wavenumber n. The Kelvin wave solutions for $s = 0$ satisfy

$$c = \pm\sqrt{gD_0}. \quad (5.2)$$

For those solutions v is zero, and u and h decay exponentially to the left of the propagation direction with decay length $|c|/f$. As previously mentioned (and demonstrated in appendix B), there is also a spurious inertial solution $c = \pm f/k$, which is shown to be invalid in appendix B. The Rossby wave solution, obtained by assuming that s is small and that c is proportional to it, is given by

$$c = -\frac{sf}{L}\frac{1}{k^2 + (n^2\pi^2/L^2) + f^2/(gD_0)}. \quad (5.3)$$

The eigensolutions in this case are sinusoidal in y. The solutions in this paper are given in dimensional form because the various waves have different scales. Most of the results are for the parameter values: $L = 5 \times 10^6$ m, $gD_0 = 4 \times 10^4$ m^2 s^{-2}, $f = 10^{-4}$ s^{-1}.

Figure 1 gives the phase speeds for the Poincaré and Kelvin modes as a function of s from 0.05 to 1.95 for $k = 2\pi/L$. The equations become singular for $s = 2$, which corresponds to zero mean depth at $y = L/2$ [see (2.11)]. All of the curves show a general decrease in speed as the s increases, and the curvature of the curves increases as s approaches 2. The gravest mode for each sign is a Kelvin wave, and the other modes are Poincaré waves with meridional wavenumbers that increase by 1 from one curve to the next.

Figure 2 gives selected positive solutions on an expanded scale along with the analytic solutions that are computed from the formulas derived by Hyde (1984). The Hyde solutions, which were obtained from an expansion in s, consist of a linear correction to the $s = 0$ analytic solutions (5.2) or (5.3). The figure shows that our curves match the $s = 0$ solutions, and they also have the same slope near $s = 0$ as predicted by Hyde. However, all of our curves depart considerably from the linear dependence as s increases. For the Kelvin wave (Fig. 2a) our complete solution begins to leave the Hyde curve for $s > 0.25$ and after $s = 0.6$, it decreases to 62% of the Hyde value at $s = 1.95$. This complex behavior is associated with a very unusual variation in the eigenfunction as a function of s, which will be shown in section 6. Figure 2b gives the first Poincaré mode: our complete solution departs from the Hyde curve for $s > 0.5$ and it increases to a maximum near $s = 1.5$ before dropping rapidly. For the

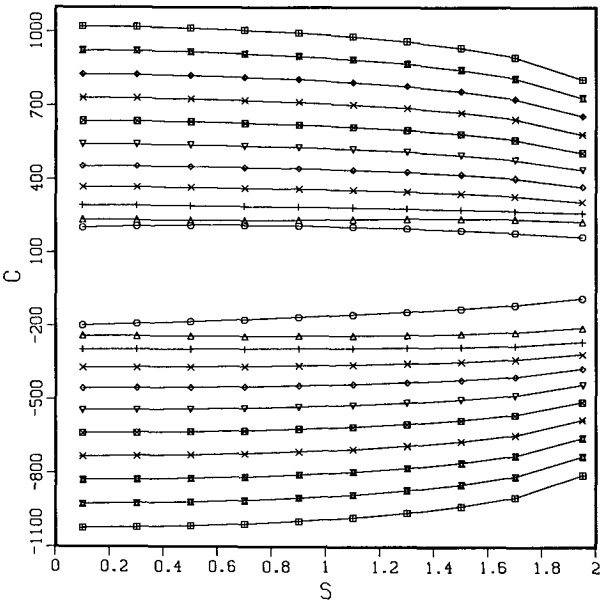

FIG. 1. Phase speeds for Poincaré and Kelvin modes as a function of s from $s = .05$ to 1.95, for $L = 5 \times 10^6$ m, $gD_0 = 4 \times 10^4$ m^2 s^{-2}, $f = 10^{-4}$ s^{-1}, $k = 2\pi/L$.

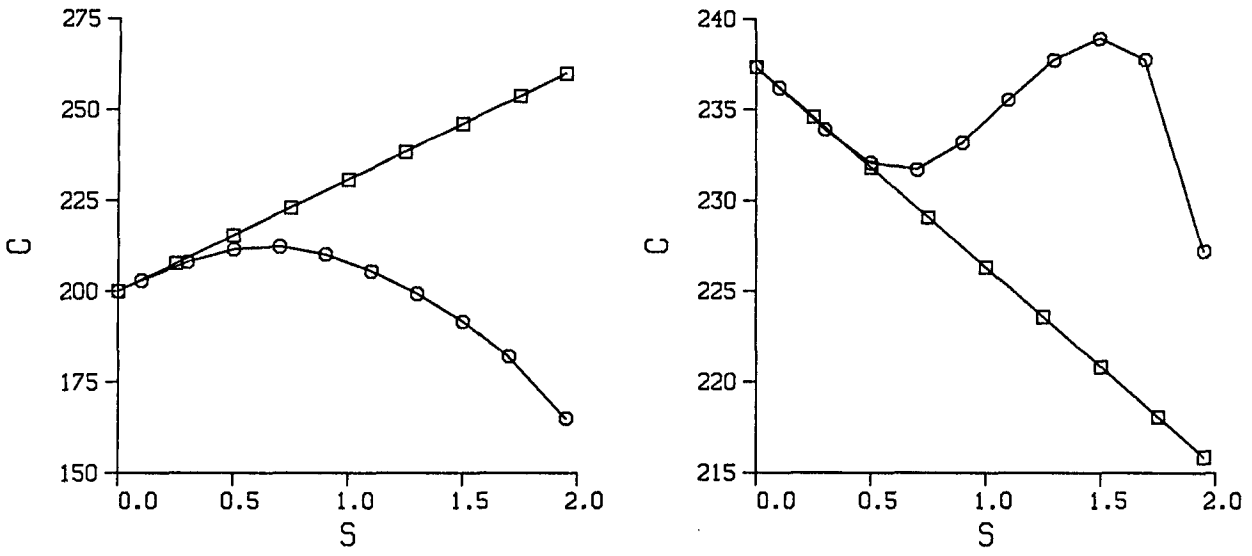

FIG. 2. Selected positive solutions from Fig. 1 compared with the Hyde solutions: (a) Kelvin wave and (b) first Poincaré mode.

higher Poincaré modes (4 and 8), which are not shown, the Hyde solutions give very little change while the complete solutions begin to drop for $s > 0.3$ and are about 20% lower at $s = 1.95$.

Figure 3 gives the negative solution comparisons for the same waves. Hyde's solutions all have the same slopes as for the positive solutions and these slopes agree with our slopes near $s = 0$. For $s > 0.25$ the complete solutions depart from the Hyde curves and move toward $c = 0$.

Figure 4 contains the phase speeds for the first 12 Rossby modes as a function of s for $k = 2\pi/L$. All of these curves are concave downward. Figure 5 compares our complete solutions with the traditional Rossby formula (5.3), obtained by linearizing the depth variation. For modes 1 and 2 in y the concave downward form of the complete solution curve leads to increased (negative) speeds as s is increased, with similar behavior for the higher modes. However, the traditional formula is quite accurate up to $s \sim 1$.

In order to determine the sensitivity of the results to the x wavenumber (k) the phase speeds are obtained for twice and one-half of the x wavelength (not shown). Except for changes in scale the Kelvin and Poincaré

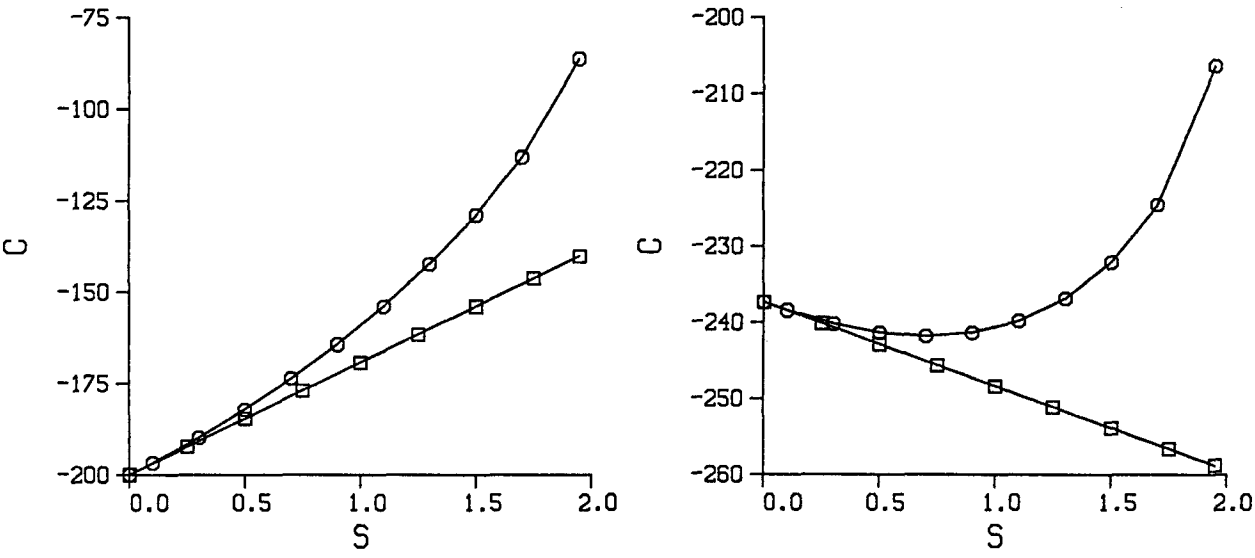

FIG. 3. Same as Fig. 2 except for negative solutions.

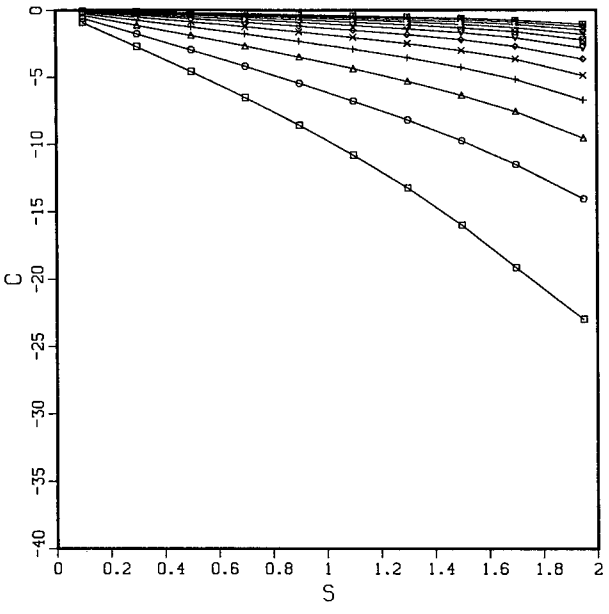

FIG. 4. Phase speeds for Rossby modes with same parameters as in Fig. 1.

waves and the Rossby waves are similar to the solutions found in Figs. 1 and 4.

A scale analysis of (2.10) shows that the solutions depend on the rotational Froude number

$$F = \frac{L^2 f^2}{gD_0}, \tag{5.4}$$

and s, provided that y, k, and c are scaled by L, L^{-1}, and $\sqrt{gD_0}$, respectively. In order to determine the solution dependence on F we replace f with $\sqrt{10}f$, which increases F by 10. Figures 6 and 7 give the phase speeds for the Kelvin and Poincaré waves and for the Rossby waves. The Kelvin and Poincaré waves (Fig. 6) are similar to those in Fig. 1. The Rossby waves (Fig. 7) have larger speeds than in Fig. 4, but the curves still have a downward curvature. When F is decreased by 10 by replacing f with $f/\sqrt{10}$ (not shown), the solutions are similar to the other cases except that the Rossby speeds are lower. Clearly, the basic behavior in s for these solutions is not strongly dependent on k or F.

The basic results given in this section (Figs. 1–5) are for the following constants:

$$L = 5 \times 10^6 \text{ m}, \quad f = 10^{-4} \text{ s}^{-1}, \quad gD_0 = 1 \text{ m}^2 \text{ s}^{-2},$$

and with these values $F = 6.25$. For the case where f is increased (Figs. 6 and 7) we obtain $F = 62.5$. The length scale in Figs. 1–5 is probably large for most atmospheric topography, but it does give a topographic beta effect, which is of the same order as the Coriolis beta effect. The region east of the Rocky Mountains could be represented by $L = 8 \times 10^5$ m. If we assume an unbounded two-layer system, then gD_0 can be replaced by $g(\Delta\theta/\theta)D_0$, where $\Delta\theta$ is the potential temperature change across the interface. If we let $\Delta\theta/\theta = 1/10$ and $D_0 = 10^3$ m, then $F = 6.4$, which is essentially the F for the solutions in Figs. 1–5. The phase speeds are the same as long as they are scaled by $\sqrt{gD_0}$.

The free-surface slope term fUL/gD_0 is equal to 1 if $L = 5 \times 10^6$ m, $f = 10^{-4}$ s^{-1}, $U = 10$ m s^{-1}, and $gD_0 = 4 \times 10^3$ m^2 s^{-2}, where the last term uses $\Delta\theta/\theta = 1/10$. In this case, $F = 62.5$, which is the value for Figs. 6 and 7. Many other reasonable combinations of parameters can be found that give rotational Froude

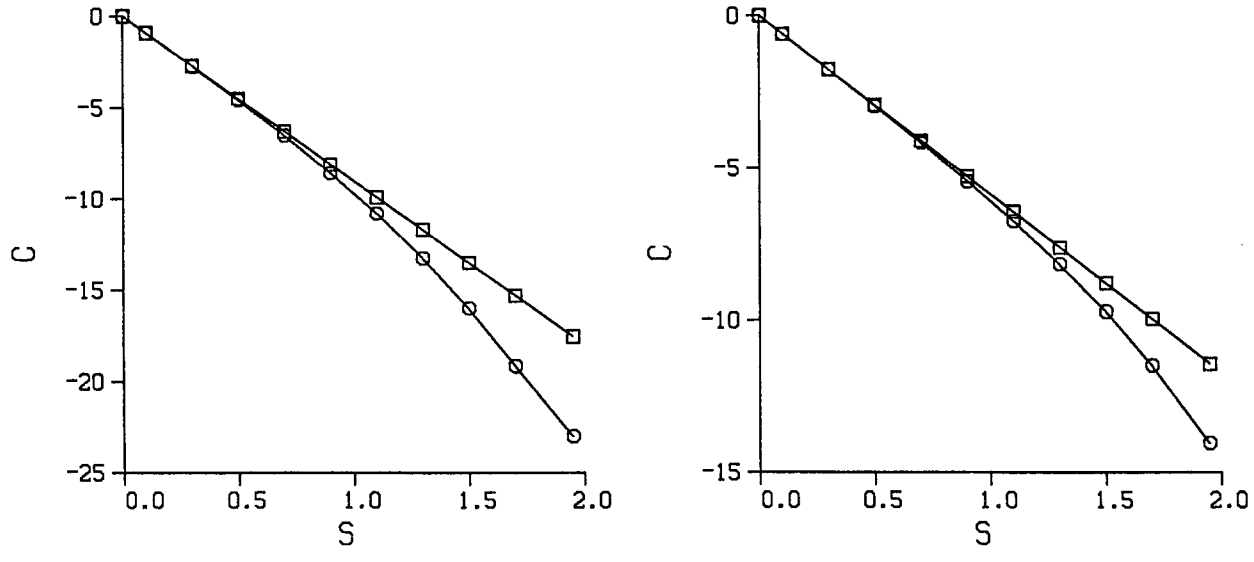

FIG. 5. Comparison of first two Rossby modes with traditional Rossby formula (5.3).

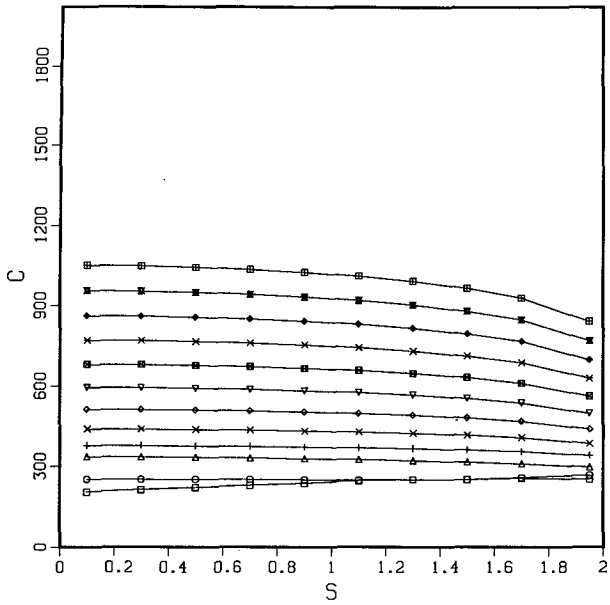

FIG. 6. Same as Fig. 1 except that $f = \sqrt{10} \times 10^{-4}\ s^{-1}$.

numbers within the range shown in these figures. The results can also be applied to the ocean by noting that $F = L^2/R^2$, where R is the Rossby radius of deformation. In the ocean L_R is often in the range 2.5–5.0 $\times 10^4$ m, so that F will be in the range considered if scale of the topography is of order 10^5 m or larger.

6. Eigenfunctions

In this section, selected eigenfunctions will be presented to illustrate the effects of finite s on the solution

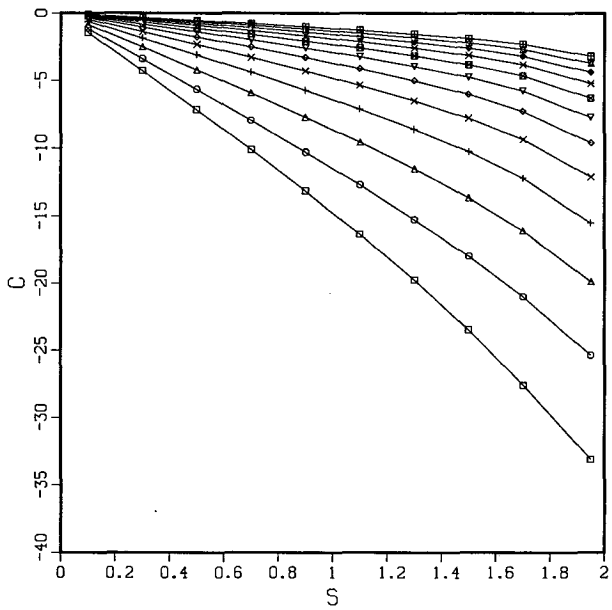

FIG. 7. Same as Fig. 4 except that $f = \sqrt{10} \times 10^{-4}\ s^{-1}$.

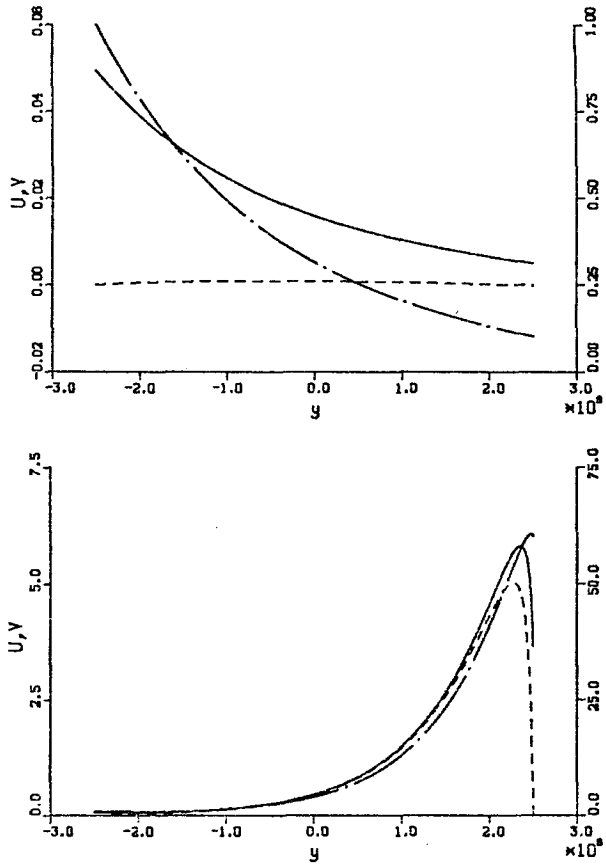

FIG. 8. Eigenstructures of positive Kelvin waves as a function of y: (a) $s = 0.1$ and (b) $s = 1.95$. The curves are labeled as u: solid, v: dotted, η: chain dot. The velocity scale is on the left, and the height scale is on the right.

structure. All of these results are for $k = 2\pi/L$ and $f = 10^{-4}\ s^{-1}$. Figure 8a gives the structure of the positive Kelvin wave for $s = 0.1$. Note that the v field is much smaller than the u field, consistent with the pure Kelvin wave ($s = 0$). The η and u fields decay exponentially away from the boundary at $y = -L/2$. The structure of the positive Kelvin wave for $s = 1.95$ is given in Fig. 8b. This solution is radically different from the pure Kelvin wave–type solution shown in Fig. 8a, because most of the disturbance is near the boundary at $y = L/2$. In this case the u and v components are of the same order, and they both have peaks near the boundary ($y = L/2$). In general, these solutions decay much more rapidly away from the boundary as compared with the solutions for $s = 0.10$.

Figure 9a contains the u field for selected values of s in order to show the evolution with increased s. The figure shows that when $s = 0.5$ the field is rather flat, although the maximum is still at $y = -L/2$. For $s > 0.7$ the maximum is near the $y = L/2$ boundary, and as s increases, the amplitude becomes more confined near this boundary. Figure 9b gives the v field for the same values of s. For $s = 0.05$ the amplitude is very small,

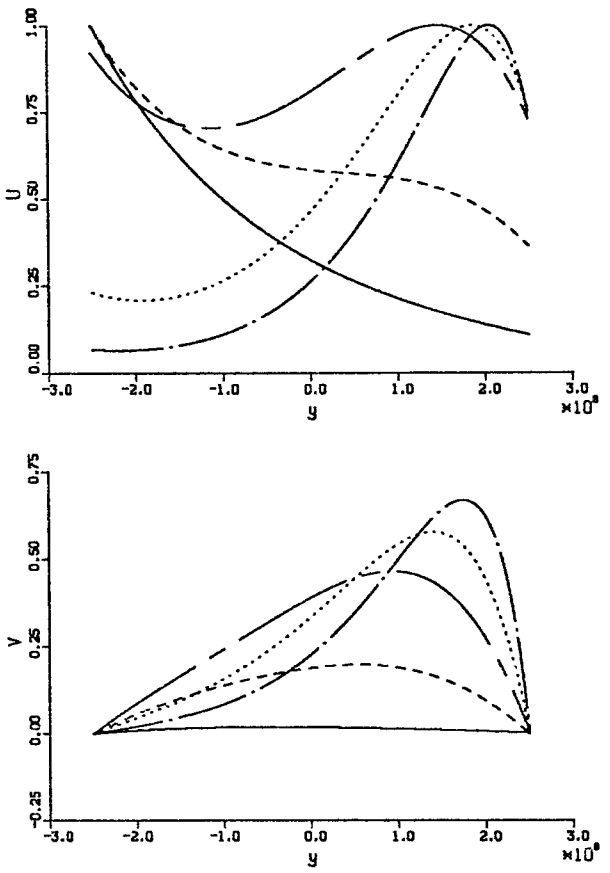

FIG. 9. (a) The u structure of the positive Kelvin wave for selected values of s. (b) The v structure for the positive Kelvin wave. The curves are labeled as solid: $s = 0.1$, dashed: $s = 0.5$, chain dashed: $s = 1.1$, dotted: $s = 1.5$, and chain dot: $s = 1.95$.

but the peak occurs for $y < 0$. As s grows the magnitude of v grows rapidly, and the peak shifts toward the wall at $y = L/2$. Although these solutions as a function of s are continuous with the pure Kelvin solution, they do not resemble the Kelvin wave for $s > 0.7$ since the maximum is near the opposite boundary and since v is the same order as u.

Figure 10a gives the structure of the negative Kelvin wave for $s = 0.1$, and it is very similar to the positive Kelvin solution (Fig. 8a) except that the maximum amplitude is at $y = L/2$. The structure of the negative Kelvin wave for $s = 1.95$ is given in Fig. 10b. The solutions damp rapidly away from the boundary at $y = L/2$, and the v field is much smaller than the u field. This solution still has the Kelvin wave structure for $s = 1.95$, unlike the solution with positive phase speed.

Figures 11a and 12a give the structure of the first and fourth positive Poincaré modes for $s = 0.1$. These are nearly sinusoidal as is the case for $s = 0$. The structure of the corresponding modes for $s = 1.95$ are found in Figs. 11b and 12b. These solutions are highly distorted with the largest amplitude and smallest y scale near $y = L/2$, where the fluid is shallowest. This behavior is closely related to the behavior of shallow-water waves as they propagate into shallow water (Stoker 1957). The mass fluxes uH_0 and vH_0 have nearly uniform wave amplitude in y. The negative Poincaré modes have similar behavior. In general, the free surface eigenfunctions for the negative Kelvin and Poincaré waves at $s = 1.95$ resemble the solutions obtained by Saint-Guily (1976). His depth field reaches 5% of the maximum depth at the edge of the shelf.

Figures 13a and 14a give the structure of the first and fourth Rossby modes for $s = 0.1$. These fields are nearly sinusoidal for this value of s. The structures of the corresponding modes for $s = 1.95$ are shown in Figs. 13b and 14b. As with the Poincaré modes, these solutions are highly distorted with the smallest y scale near $y = L/2$. Also note that u is larger than v, consistent with the large η gradient near the boundary if u and v are approximately geostrophic.

The eigenmode dependence on s for the Rossby waves can be explained with the following approximate formula for the Rossby-wave frequency

$$\sigma = -\frac{D_0}{H_0}\frac{sf}{L}\frac{k_x}{k_x^2 + k_y^2 + (f^2/gH_0)}, \qquad (6.1)$$

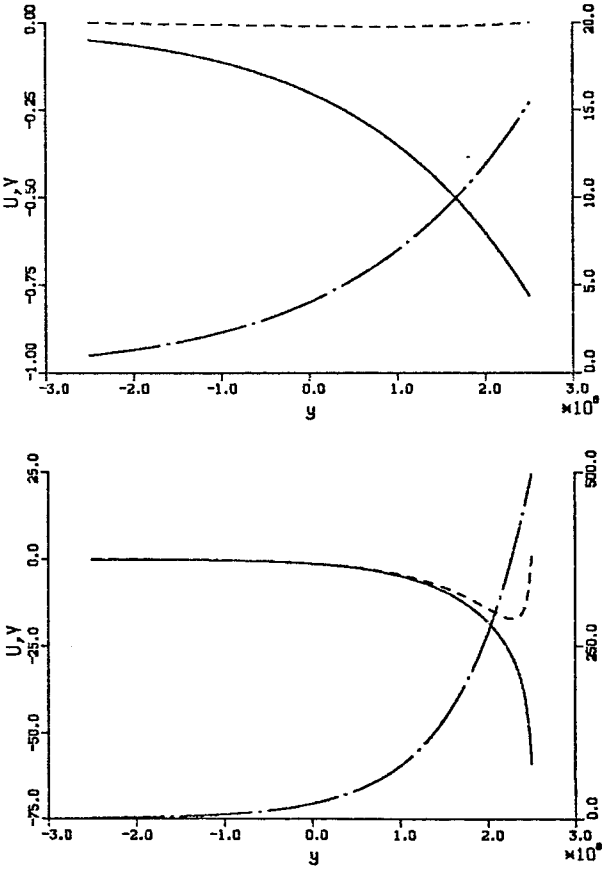

FIG. 10. Same as Fig. 8 except for negative Kelvin wave.

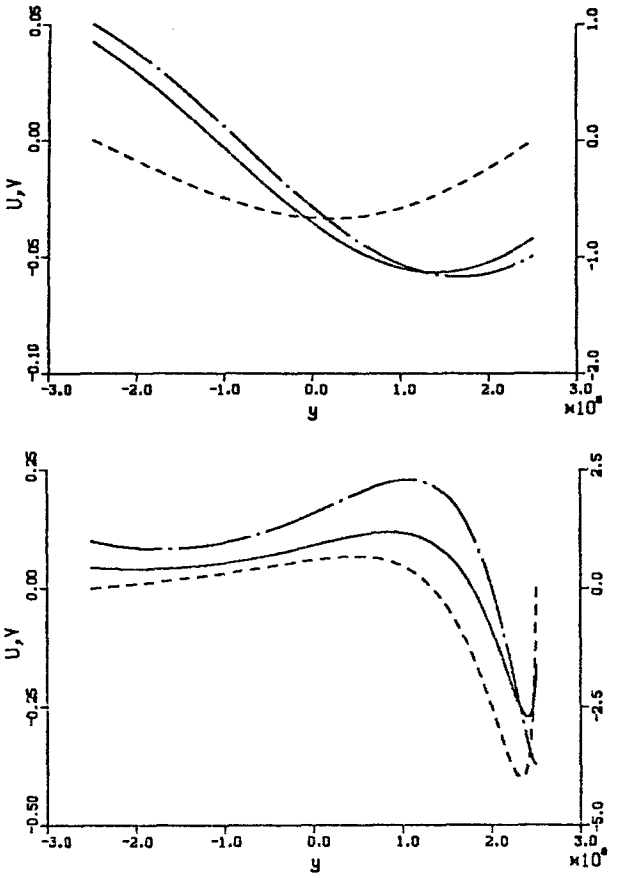

FIG. 11. Same as Fig. 8 except for first positive Poincaré mode.

where k_x is the x wavenumber and k_y is the y wavenumber. The waves in this paper are actually pairs of plane waves that are summed to satisfy the boundary conditions. As the plane waves propagate toward lower values of H_0, k_y must change to keep the frequency constant since $k_x = k$ does not change. Equation (6.1) shows that as $1/H_0$ increases, k_y^2 must also increase, which gives the short y scales observed near $y = L/2$.

7. Conclusions

In this paper, we solve the linearized shallow-water equations in a channel with a linear depth variation and or a linear free surface variation if a mean current is present. The solutions are obtained in terms of confluent hypergeometric functions. In order to check the solutions over the proper range of $a(c)$, a very high resolution finite-difference numerical model is also solved. It turns out that the numerical solution is computationally less intensive.

The phase speeds are computed for a range in s from 0.1 to 1.95. The equations become singular for $s = 2.0$ when the depth at $y = L/2$ becomes zero. For small s the Kelvin and Poincaré solutions agree with the solutions obtained by Hyde (1984) with a perturbation expansion in s. However, for $s > 0.25$ the solutions depart considerably from the Hyde solutions, which are linear in s. For $s > 1.0$ the magnitudes of the phase speeds decrease as s increases up to $s = 1.95$. The Rossby wave phase speed is close to the approximate speed obtained when the depth is linearized. Beyond $s \sim 1$ the complete solutions become concave down so that the speed is increased relative to the simple formula.

For small s the eigenfunctions of the Kelvin and Poincaré waves are very close to the $s = 0$ solutions (i.e., exponential for Kelvin waves and sinusoidal for Poincaré waves). However, as s increases to $s = 1.95$, the eigenfunctions are distorted so that the largest amplitude and smallest scale occur near the boundary where the depth is least ($y = L/2$). The most remarkable change is for the positive Kelvin wave that begins for small s with u and η decaying exponentially from the boundary at $y = -L/2$ and $v \sim 0$. As s increases the maxima shift across the channel and v approaches u in magnitude. For $s = 1.95$ these solutions resemble the negative Kelvin wave except that v is large and it propagates in the positive direction. This solution is,

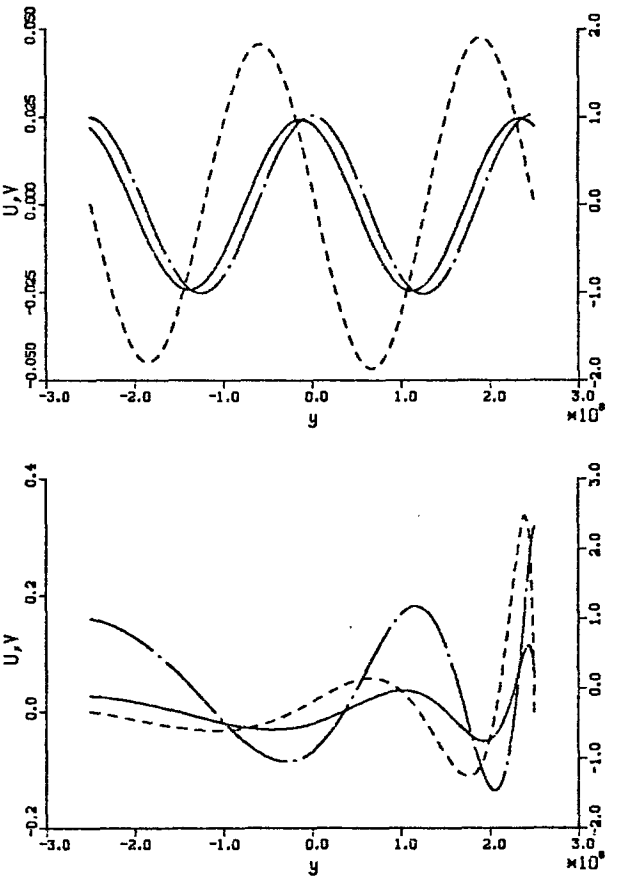

FIG. 12. Same as Fig. 8 except for fourth positive Poincaré mode.

however, consistent with the other solutions that are highly confined near $y = L/2$ as s approaches 2. The negative Kelvin wave retains the Kelvin wave structure as s increases to 1.95. The latter solutions decay more rapidly away from the boundary on the shallow side of the channel ($y = L/2$). The decrease in $|c|$ as s increases can now be interpreted in terms of the eigenfunction structure shift toward the boundary where the depth is the least. In Eqs. (5.1) and (5.2) it can be seen that the phase speed decreases as the depth D_0 decreases. Thus, as the depth decreases at the point where the wave has a maximum amplitude, we would expect the phase speed to decrease as observed. The Rossby wave eigenfunctions also show a shift so that the amplitude increases and the y scale decreases near the boundary where the fluid is shallow. This scale decrease is explained with frequency formula (6.1). This formula also shows that the phase speed will increase as the local depth H_0 is decreased as is observed.

The results in this paper can be applied to a variety of simplified situations in the atmosphere and the ocean by changing the scale and employing a reduced gravity in a two-layer system.

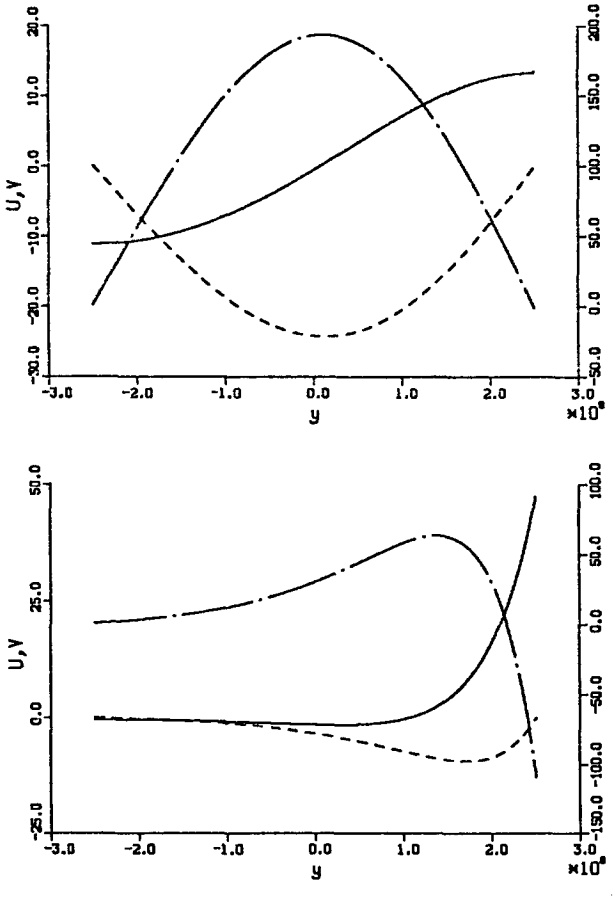

FIG. 13. Same as Fig. 8 except for first Rossby mode.

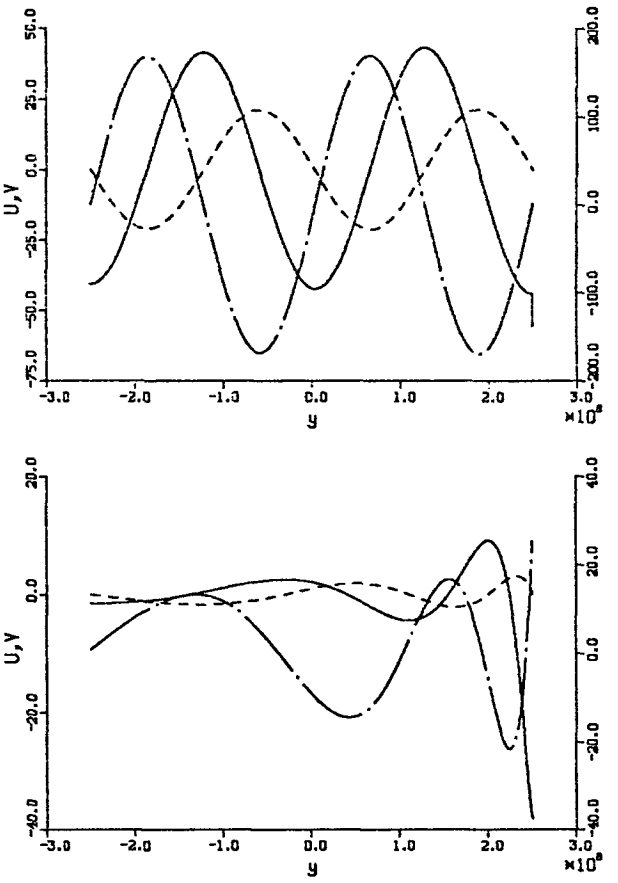

FIG. 14. Same as Fig. 8 except for fourth Rossby mode.

Acknowledgments. We would like to thank the late Professor L.-O. Merkine and Professor J. A. Cochran for helpful discussions on this research. We also thank Professor J. Pryce for obtaining the positive eigenvalues independently using NAG software library, and Professor W. Gragg for developing the subroutines to compute the confluent hypergeometric functions. The manuscript was carefully typed by Mrs. P. Jones, and the numerical calculations were carried out at the W. R. Church Computer Center of the Naval Postgraduate School. This paper was prepared in part for the Office of Naval Research. Funding was provided by the Naval Postgraduate School.

APPENDIX A

Proof that c is Real

Let

$$u = u(y) \exp[ik(x - ct)], \qquad (A.1)$$

and similarly for v and η. Substitution of these expressions into (2.2)–(2.4) yields

$$-ikcu = fv - ikg\eta, \qquad (A.2)$$

$$-ikcv = -fu - g\frac{d\eta}{dy}, \tag{A.3}$$

and

$$-ikc\eta = -ikH_0u - \frac{d}{dy}(H_0v). \tag{A.4}$$

Multiplying (A.2)–(A.4) by $H_0\bar{u}$, $H_0\bar{v}$, and $g\bar{\eta}$, respectively, where $\bar{(\ )}$ denotes complex conjugation and summing gives

$$-ick\{H_0[|u|^2 + |v|^2] + g|\eta|^2\} = -H_0\left[f(u\bar{v} - \bar{u}v) + ikg(u\bar{\eta} + \bar{u}\eta) + g\bar{v}\frac{d\eta}{dy}\right] - g\bar{\eta}\frac{d}{dy}(H_0u). \tag{A.5}$$

Summing (A.5) with its complex conjugate and integrating from $y = -L/2$ to $y = +L/2$ yields

$$ik(c - \bar{c})\int_{-L/2}^{L/2}\{H_0[|u|^2 + |v|^2] + g|\eta|^2\}dy = [-gH_0(v\bar{\eta} + \bar{v}\eta)]|_{y=-L/2}^{y=L/2}. \tag{A.6}$$

Since the right-hand side of (A.6) is zero (by virtue of the boundary condition that v vanish on $y = \pm L/2$) and the integral is positive definite, it follows that c is real and the solutions are neutrally stable.

APPENDIX B

Conditions for the Existence of Inertial Oscillations of the Frequency $c = \pm f/k$

Substituting $c = \pm f/k$ into (A.2)–(A.4) yields

$$fu = \pm ifv \pm kg\eta, \tag{B.1}$$

$$fu = \pm ifv - g\frac{d\eta}{dy}, \tag{B.2}$$

and

$$\pm if\eta + H_0\left(iku + \frac{dv}{dy}\right) + v\frac{dH_0}{dy} = 0. \tag{B.3}$$

The present analysis follows that of Pedlosky (1979, pp. 79–80), except that we also include the term vdH_0/dy in (B.3), which is a consequence of the depth variation. Thus, the analysis reduces to that of Pedlosky (1979) when $H_0 = \text{const}$.

It follows from (B.1) and (B.2) that

$$\eta = \eta_0 \exp(\mp ky), \tag{B.4}$$

where η_0 is a constant to be determined. Substituting (B.4) in (B.1) gives

$$u = \pm iv \pm \frac{kg}{f}\eta_0 \exp(\mp ky), \tag{B.5}$$

and substituting (B.4) and (B.5) into (B.3) yields a first-order differential equation for v; namely,

$$\frac{dv}{dy} + \left(\frac{1}{H_0}\frac{dH_0}{dy} \mp k\right)v = \pm if\eta_0\left(\frac{1}{H_0} - \frac{k^2g}{f^2}\right)\exp(\mp ky). \tag{B.6}$$

The general solution of (B.6), for the linear variation of H_0 with y defined in (2.8), is given by

$$v = \frac{\exp(\pm ky)}{1 - (s/L)y}V_0 - \frac{if}{2kD_0(1 - (s/L)y)}\eta_0 \times\left[1 - k^2R^2\left(1 - \frac{s}{L}y\right) \pm R^2\frac{sk}{2L}\right] \times \exp(\mp ky), \tag{B.7}$$

where $R = \sqrt{gD_0}/f$ is the Rossby radius of deformation.

Applying the boundary condition that $v = 0$ on $y = \pm L/2$ in (B.7) yields

$$\exp\left(\pm\frac{kL}{2}\right)V_0 - \frac{if}{2kD_0}\left[1 - k^2R^2\left(1 - \frac{s}{2}\right) \pm R^2\frac{sk}{2L}\right] \times \exp\left(\mp\frac{kL}{2}\right)\eta_0 = 0, \tag{B.8}$$

$$\exp\left(\mp\frac{kL}{2}\right)V_0 - \frac{if}{2kD_0}\left[1 - k^2R^2\left(1 + \frac{s}{2}\right) \pm R^2\frac{sk}{2L}\right] \times \exp\left(\pm\frac{kL}{2}\right)\eta_0 = 0. \tag{B.9}$$

Equations (B.8) and (B.9) will have nontrivial solutions for V_0 and η_0 provided the determinant vanishes, that is:

$$\pm\left[1 - k^2R^2 \pm R^2\frac{sk}{2L}\right]\frac{\sinh kL}{kL} = \frac{kR^2s}{2}\cosh kL. \tag{B.10}$$

Thus, the only possible inertial oscillations of frequency $c = \pm f/k$ are those for which k satisifies (B.10). When $s = 0$ we recover the degenerate inertial oscillation of Pedlosky (1979, pp. 79–80), for which $k = \pm R^{-1}$, and it is indistinguishable from the Kelvin wave, for which $v = 0$.

REFERENCES

Abramowitz, M., and I. A. Stegun, 1965: *Handbook of Mathematical Functions.* Dover Pub., 1046 pp.

Hyde, R. A., 1984: The influence of variable rotation and variable depth on barotropic Kelvin and Poincaré waves. *J. Atmos. Sci.*, **41**, 38–50.

Pedlosky, J., 1979: *Geophysical Fluid Dynamics.* Springer Verlag, 710 pp.

Robinson, A. R., 1964: Continental shelf waves and the response of sea level to weather systems. *J. Geophys. Res.*, **69**, 367–368.

Saint-Guily, B., 1976: Sur la propagation des ondes de seconde classe le long d'un talus continental, *C. R. Acad. Sci. Paris*, **282**, 269–272.

Stakgold, I., 1979: *Green's Functions and Boundary Value Problems.* Wiley, 638 pp.

Stoker, J. J., 1957: *Water Waves.* Interscience, 567 pp.

Wimp, J., 1984: *Computation with Recurrence Relations.* Pitman Advanced Publishing Program, 310 pp.